# Failure behavior of single sand grains: Theory versus experiment

R. H. Brzesowsky,[1,2] C. J. Spiers,[1] C. J. Peach,[1] and S. J. T. Hangx[1,3]

Received 24 November 2010; revised 7 March 2011; accepted 22 March 2011; published 17 June 2011.

[1] Grain-scale brittle fracture and grain rearrangement play an important role in controlling the compaction behavior of reservoir rocks during the early stages of burial. Therefore, the understanding of single-grain failure is important. We performed constant displacement rate crushing tests carried out on selected, well-rounded, single sand grains and on randomly sampled grains from different grain size ($d$) batches of pure quartz sand. Applying a Hertzian fracture mechanics model for grain crushing, the critical load at failure ($F_c$) data obtained for the selected grains were converted into an accurate estimate of the size of flaws associated with failure ($c_f$). Similarly, the distributed $F_c$ data obtained from the different batch samples were converted into distributions of grain failure stress. Weibull weakest link theory could not explain the observed grain failure behavior. On the contrary, the Hertzian grain failure criterion enabled the conversion of the distributed $F_c$ data, for the batch samples, into distributions of $c_f$, assuming spherical grains, or of "effective" radius of curvature ($r_g$), characterizing contact surface asperities in the case of nonspherical grains. In contrast to the model of Zhang et al. (1990), our work shows that there is no clear physical basis for a grain size dependence of $c_f$. However, since roundness data for dune sands exhibit a similar relation between $r_g$ and $d$, as seen in our grain size batches, it is inferred that the Hertzian fracture mechanics model assuming nonspherical grains with a distributed $r_g$ is the most physically reasonable model for grain failure.

**Citation:** Brzesowsky, R. H., C. J. Spiers, C. J. Peach, and S. J. T. Hangx (2011), Failure behavior of single sand grains: Theory versus experiment, *J. Geophys. Res.*, *116*, B06205, doi:10.1029/2010JB008120.

## 1. Introduction

[2] Experimental and microstructural studies show that grain-scale brittle fracture plus grain rearrangement play an important role in controlling the compaction behavior of high-porosity sandstones and sands under upper crustal conditions during the early stages of burial [*Antonellini et al.*, 1994; *Burley*, 1986; *Chester et al.*, 2004; *Chuhan et al.*, 2003; *Groshong*, 1988; *Wilson and McBride*, 1988; *Wu and Groshong*, 1991]. Grain-scale fracture and rearrangement are believed to be mechanisms of importance in controlling the porosity and permeability evolution of sedimentary rocks in rapidly subsiding basin settings [*Chuhan et al.*, 2002, 2003; *Donaldson et al.*, 1995]. They may also be of importance in controlling production-related compaction of hydrocarbon reservoir rocks, as a result of rapidly changing effective stresses, leading to surface subsidence [*Doornhof et al.*, 2006; *Hettema et al.*, 2002; *Schutjens et al.*, 1994; *Zoback and Byerlee*, 1976].

[3] A theoretically and experimentally based understanding of these mechanisms is needed in order to develop micromechanical models that can eventually be used in macroscale modeling of both upper crustal deformation and the compaction of clastic hydrocarbon reservoirs in the (post)production phase. As an integral step in this direction, an understanding of single-grain failure behavior is essential. Experimental studies on time-independent compaction of porous sandstones and sands at room temperature have shown irrecoverable porosity reduction during loading, which increases significantly beyond a specific critical effective pressure ($P_{cr}$) [*Borg et al.*, 1960; *Chuhan et al.*, 2003; *Dunn et al.*, 1973; *Karner et al.*, 2003, 2005; *Lambe and Whitman*, 1969; *Lee and Farhoomand*, 1967; *McDowell and Humphreys*, 2002; *Nakata et al.*, 2001; *Vesíc and Clough*, 1968; *Wissler and Simmons*, 1985; *Wong and Baud*, 1999; *Zhang et al.*, 1990; *Zoback and Byerlee*, 1976]. Experiments on sand aggregates and sandstones have shown that the amount of compaction obtained at a given effective pressure generally increases with increasing porosity ($\varphi$) and increasing grain size ($d$) [*Borg et al.*, 1960; *Chuhan et al.*, 2002, 2003; *Dunn et al.*, 1973; *Hangx et al.*, 2010; *Karner et al.*, 2005; *Lambe and Whitman*, 1969; *Lee and Farhoomand*, 1967; *McDowell and Humphreys*, 2002; *Nakata et al.*, 1999; *Vesíc and Clough*, 1968; *Zhang et al.*, 1990]. This is in accordance with the observation that with increasing porosity and grain size, the critical pressure for grain crushing $P_{cr}$ decreases, i.e., the rock becomes weaker [*Karner et al.*, 2005; *Wong and Baud*, 1999; *Zhang et al.*, 1990]. However, it

[1]High Pressure and Temperature Laboratory, Faculty of Geosciences, Utrecht University, Utrecht, Netherlands.
[2]Now at Philips Research, Eindhoven, Netherlands.
[3]Now at Shell Global Solutions International, Rijswijk, Netherlands.


0148-0227/11/2010JB008120

should be noted that some of the above mentioned compaction experiments are performed at stress conditions below the critical crushing pressure. At the same time, crushing tests conducted on single sand grains show an increase in the load at failure ($F_c$ = 30–350 N) with increasing grain size ($d$ = 0.5–6.3 mm) [*Gallagher*, 1976; *McDowell*, 2002]. With regard to microscale failure mode, petrographic studies have revealed that the dominant grain failure mechanism leading to aggregate compaction and single-grain crushing is the development of tensile intra and transgranular cracks at grain contacts due to point loading [*Bernabe and Brace*, 1990; *Chester et al.*, 2004; *Chuhan et al.*, 2002; *Gallagher et al.*, 1974; *Gallagher*, 1976, 1987; *Gill et al.*, 1990; *Hangx et al.*, 2010; *Karner et al.*, 2003; *Myer et al.*, 1992; *Wong*, 1990; *Zhang et al.*, 1990].

[4] Compaction of porous rock by grain crushing under hydrostatic states of stress has been (micromechanically) modeled using Hertzian contact theory [*Hertz*, 1896] and linear elastic fracture mechanics (LEFM) [*Lawn*, 1993]. Previously, this approach was used to describe the hydrostatic compaction behavior of cemented porous rock, such as sandstone, by deriving an expression for the critical effective pressure for the onset of grain crushing ($P_{cr}$) as a function of porosity and flaw size [*Wong*, 1990; *Zhang et al.*, 1990].

[5] However, the model derived by Wong and coworkers [*Wong*, 1990; *Zhang et al.*, 1990] does not in itself lead to a strictly defined whole-grain failure criterion, as the porosity and grain size dependence of the critical effective pressure observed in compaction experiments is introduced to the model by relating the grain failure load to $P_{cr}$ on the basis of a random packing model and by assuming that the flaw dimension (at failure) scales linearly with grain size [see *Zhang et al.*, 1990, equation 7]. In addition, this criterion does not directly offer an explanation for the grain size dependence of the grain failure load obtained from compaction experiments and single-grain crushing tests. To apply a whole-grain failure criterion to sand grains in practice, data are needed on the dimension of flaws associated with failure ($c_f$). It should be noted though that experiments on sands and sandstones [*Karner et al.*, 2005; *Wong et al.*, 1997; *Wong and Baud*, 1999; *Zhang et al.*, 1990] show that the measured critical effective pressure for grain crushing $P_{cr}$ is in good agreement with the model presented by *Zhang et al.* [1990], even with the simple scaling between flaw size and grain size proposed in their model. Though this model appears to fit for grain aggregates, it has not been shown yet to also apply to single grains.

[6] We developed a Hertzian/LEFM-based micromechanical model for grain crushing, predicting the critical force at failure ($F_c$) to be a function of grain size (or contact surface curvature) and (surface) flaw size. Combining Weibull weakest link theory with the grain failure criterion enables us to formulate a complementary statistical model for grain crushing. This complementary model demonstrates that a purely statistical grain size effect upon grain failure probability can influence the grain size dependence of the failure stress. The applicability of both models is tested by comparison with diametric compression experiments performed on single sand grains. Results are reported of crushing tests carried out (a) on selected, well-rounded grains, and (b) on randomly sampled grains from four different grain size batches.

## 2. Micromechanical Model for Grain Crushing

[7] In the following, we introduce the basics of the Weibull weakest link theory. Then we go on to develop two micromechanical models for single-grain failure under conditions of diametric compression between flat platens. The first model consists of a grain failure criterion, adopting Hertzian contact theory and LEFM, while the second is a statistical model for single-grain failure, incorporating Weibull weakest link theory.

### 2.1. Background on Weibull Weakest Link Theory

[8] In materials science it has been long recognized that the failure stress or strength of brittle materials tested under nominally identical experimental conditions is a statistically distributed quantity. It is common practice to describe the strength and flaw size characteristics of such materials using Weibull statistics [*Jayatilaka and Trustrum*, 1977; *Kittl and Diaz*, 1988; *Lamon*, 1988; *Lawn*, 1993; *Weibull*, 1951].

[9] The Weibull theory is based on the principle that the strength of a structure is determined by its weakest component or link, and is referred to as the weakest link theory. In the case of surface flaws, a solid component with total surface area $A_{tot}$, subjected to an applied stress field, is expected to be composed of solid elements with an elementary surface area $A_0$. By analogy, volume flaws are represented by the total volume $V_{tot}$ and elementary volume $V_0$. The bulk strength of the material is dependent on the weakest, hence biggest, flaw, and thus depends on the extreme tail of the flaw size distribution. This inherently suggests that the larger the solid component, the more likely a weaker flaw will be encountered. Statistically speaking, this means that with increasing size, the material strength goes down, which is referred to as the statistical size effect of the Weibull theory [*Bazant et al.*, 1991; *Kittl and Diaz*, 1988; *Weibull*, 1951].

[10] In the original Weibull theory, the flaws within the solid elements are considered to be only affected by tensile failure, to be randomly oriented and uniformly distributed with respect to both their spatial location and orientation, and that their population is invariant in time. Moreover, the weakest link formulation assumes the solid elements to be stochastically independent and mutually exclusive, i.e., purely random and nonoverlapping. Finally, elemental failure is assumed to occur independently, meaning without mechanical interaction between elements, and with equal probability. Material failure is thus characterized by unstable catastrophic flaw propagation throughout the bulk of the solid, independently of the strength of the other elements encountered on the crack path [*Batdorf and Crose*, 1974; *Batdorf and Heinisch*, 1978; *Bazant et al.*, 1991; *Chao and Shetty*, 1990; *Lamon*, 1988; *Matthews et al.*, 1976; *Quinn and Morrell*, 1991; *Scholten*, 1993].

[11] Fracture mechanics theory predicts that material failure occurs if the equivalent stress intensity factor $K_{eq}$ exceeds a critical level equal to the equivalent fracture toughness $K_{c,eq}$ [e.g., *Lawn*, 1993]. This general failure criterion can be expressed as [e.g., *Thiemeier et al.*, 1991]

$$K_{eq} = Y\sigma_{eq}\sqrt{\pi c} \geq K_{c,eq} \quad (1)$$

where $\sigma_{eq}$ is the scalar representation of the tensorial state of stress acting on a typical flaw, defined in terms of the flaw orientation and normal or shear stresses acting on the flaw, and $Y$ is a dimensionless factor dependent on the geometry of the structure and the shape of the flaw.

[12] For a brittle material, the probability that the failure stress or strength of the material is less than or equal to the applied equivalent stress $\sigma_{eq}$ is equal to the probability that the material contains a flaw with a size larger than or equal to the critical size $c_f$. Accordingly, the Weibull failure probability of the solid ($P_f$) [see, e.g., *Chao and Shetty*, 1990; *Fok and Smart*, 1993; *Smart and Fok*, 1994], is expressed as

Surface flaws

$$P_f = 1 - \exp\left[-\frac{1}{A_0}\int_{A_{tot}}\frac{1}{2\pi}\int_0^{2\pi}\left(\frac{\sigma_{eq}}{\sigma_{ch}}\right)^m d\theta\, dA_0\right] \tag{2a}$$

Volume flaws

$$P_f = 1 - \exp\left[-\frac{1}{V_0}\int_{V_{tot}}\frac{1}{4\pi}\int_0^{2\pi}\int_0^{\pi}\left(\frac{\sigma_{eq}}{\sigma_{ch}}\right)^m \cos\theta\, d\theta\, d\psi\, dV_0\right] \tag{2b}$$

where $\sigma_{ch}$ is the characteristic strength and $m$ is the Weibull modulus.

[13] The value of the equivalent stress is dependent on the choice of failure criterion. Such criteria can include the principal stresses acting on the flaw (principle of independent action (PIA)) [e.g., *Stanley et al.*, 1973], the normal stress acting on the flaw (normal stress averaging (NSA)) [*Weibull*, 1951], or the maximum coplanar energy release rate (GMAX) [*Hellen and Blackburn*, 1975]. In particular, the last mentioned would give a more general description of failure. However, for practical use of the failure probability function, it is desirable to express the equivalent stress in terms of an externally applied load or a typical, measurable stress. To this extent, the nominal stress $\sigma_{nom}$ is introduced, which is defined as the maximum tensile stress within the specimen or solid. Accordingly, the expression for the failure probability function becomes

Surface flaws

$$P_f = 1 - \exp\left[-\frac{A_{tot}}{A_0}\left(\frac{\sigma_{nom}}{\sigma_{ch}}\right)^m\left(\int_{A_{tot}}\frac{1}{2\pi}\int_0^{2\pi}\left(\frac{\sigma_{eq}}{\sigma_{nom}}\right)^m d\theta\, d\frac{A_0}{A_{tot}}\right)\right] \tag{3a}$$

Volume flaws

$$P_f = 1 - \exp\left[-\frac{V_{tot}}{V_0}\left(\frac{\sigma_{nom}}{\sigma_{ch}}\right)^m\left(\int_{V_{tot}}\frac{1}{4\pi}\int_0^{2\pi}\int_0^{\pi}\left(\frac{\sigma_{eq}}{\sigma_{ch}}\right)^m \cdot \cos\theta\, d\theta\, d\psi\, d\frac{V_0}{V_{tot}}\right)\right] \tag{3b}$$

A stress integral $\Phi(A_{tot})$ or $\Phi(V_{tot})$, respectively, can be introduced, which is a dimensionless parameter only dependent on the shape of the specimen or solid, and is defined as

Surface flaws

$$\Phi(A_{tot}) = \int_{A_{tot}}\frac{1}{2\pi}\int_0^{2\pi}\left(\frac{\sigma_{eq}}{\sigma_{nom}}\right)^m d\theta\, d\frac{A_0}{A_{tot}} \tag{4a}$$

Volume flaws

$$\Phi(V_{tot}) = \int_{V_{tot}}\frac{1}{4\pi}\int_0^{2\pi}\int_0^{\pi}\left(\frac{\sigma_{eq}}{\sigma_{ch}}\right)^m \cos\theta\, d\theta\, d\psi\, d\frac{V_0}{V_{tot}} \tag{4b}$$

Furthermore, we can define the Weibull scale parameter $k$ as

$$k = \sigma_{ch}\left(\frac{Z_0}{Z_{tot}\Phi(Z_{tot})}\right)^{1/m} \tag{5}$$

where the general measures $Z_{tot}$ and $Z_0$ are introduced, which represent $V_{tot}$ or $A_{tot}$ and $V_0$ or $A_0$, respectively, as expressed in equations (3) and (4). As a result, the expression for the Weibull failure probability as a function of the nominal stress (equation (2)) reduces to a two-parameter form as given as

$$P_f(\sigma_{eq}) = 1 - \exp\left[-\left(\frac{\sigma_{nom}}{k}\right)^m\right] \tag{6}$$

Note that when $\sigma_{nom} = k$ at failure, the failure probability $P_f$ is equal to $1 - e^{-1} \approx 0.63$, regardless of the value of $m$.

### 2.2. Grain Failure Criterion

[14] We now describe the failure of a grain loaded diametrically between two flat platens. We do this by applying a normal stress averaging criterion, in the form of the Hertzian contact stress, to represent the equivalent stress acting on the flaw. Both solids are assumed to be elastic and to make idealized Hertzian contact. According to Hertzian contact theory for solids of revolution, the radius ($a$) of the contact circle between a grain ($g$), with a spherical precontact surface, and a flat plate ($p$), with an infinite radius of curvature $R_p$, is given by the relation [*Johnson*, 1987]

$$a^3 = \frac{3FR_f}{4E^*} = \frac{3FR_g}{4}\left[\frac{\left(1-\nu_g^2\right)}{E_g} + \frac{\left(1-\nu_p^2\right)}{E_p}\right] \tag{7}$$

Within a cylindrical coordinate reference frame, the Hertzian radial stress $\sigma_{rr}$ within the contact reaches a maximum tensile value at the edge of the circular contact area, given as

$$\sigma_T = (1 - 2\nu_g)\sigma_0/3 \tag{8}$$

where $\sigma_0 = 3F/2\pi a^2$ is the normal stress at the center of the contact [*Huber*, 1904].

[15] We assume that the grain surfaces contain preexisting, Griffith-type, surface flaws of initial dimension $c_0$. Furthermore, if the radius of the contact circle and the initial flaw size are much smaller than the grain radius of curvature, Hertzian and LEFM theory predict that a tangentially aligned flaw at the edge of the contact can be considered as a straight single-ended (edge) crack in an elastic half-space subjected to an equivalent stress $\sigma_{eq}$. In our model, we assume that the crack will remain unstable along its advancement path, causing instantaneous, catastrophic grain failure.

[16] Combining equations (1) and (7) for the fracture toughness and contact radius, with the definitions for tensile stress (equation (8)) and normal stress at the contact yields the critical force at failure ($F_c$), for a grain with initially spherical contact surface, given as

$$F_c = \frac{9\pi\sqrt{\pi}K_{c,eq}^3 R_g^2}{2c_f\sqrt{c_f}Y^3(1-2\nu_g)^3(E^*)^2} \quad (9)$$

As can be seen, this equation is very similar to the one proposed by *Zhang et al.* [1990], which served as the basis for our equation. In comparison, our equation contains an $E^*$ term, instead of $E$, where $E^*$ represents the combined elastic properties of the grain and the substrate platen, defined as $E^* = \frac{(1-\nu_g)}{E_g} + \frac{(1-\nu_p)}{E_p}$. For two spherical grains $\nu_g = \nu_p$ and $E_g = E_p$, which reduces the above equation to *Zhang et al.* [1990, equation 4].

[17] A similar exercise can be performed for a grain with an initially ellipsoidal surface, using the appropriate equations for $\sigma_T$ and $\sigma_0$, and the assumptions for a grain flat platen contact, as given by *Johnson* [1987], resulting in

$$F_c \approx \frac{\pi\sqrt{\pi}K_{c,eq}^3(R_g')^3}{6c_f\sqrt{c_f}Y^3(1-2\nu_g)^3(E^*)^2(R_g'')} \frac{q_e^3\sqrt{q_e}}{\tanh^{-1}[\sqrt{q_e}] - \sqrt{q_e}} \quad (10)$$

From the model for spherical grain contact surfaces (i.e., equation (9)), it is clear that in the case of spherical grains with a grain size $d = 2R_g$ and a fixed narrow flaw size distribution, the grain failure load $F_c$ is proportional to $R_g^2$, in other words $F_c \propto d^2$. Conversely, for a given population of grains with distributed values of flaw size or grain radius of curvature, including varying asperity radius, $F_c$ will also be a distributed quantity.

### 2.3. Weibull Model for Grain Failure

[18] Application of the Weibull weakest link theory to single-grain failure is now attempted, broadly following *Kschinka et al.* [1986], assuming that individual grains are spherical and can hence be represented by their grain volume, $V_{tot} = 4\pi R_g^3/3$, or surface area, $A_{tot} = 4\pi R_g^2$, in the Weibull failure probability equations (cf. section 2.1). Now, considering grain failure to initiate at either volume or surface flaws, located within the effective grain volume $V_{eff} = \gamma_V V_{tot}$ or surface area $A_{eff} = \gamma_A A_{tot}$ (where $\gamma_V$ and $\gamma_A$ are scaling factors) and subjected to a locally uniform and constant tensile stress field, the Weibull model for uniaxial stress can be applied. Accordingly, the nominal stress at failure ($\sigma_{f,nom}$) of an individual grain exhibits a clear grain size dependence if equations (5) and (6) are written in the form

$$\sigma_{f,nom} = \sigma_{ch}\left(-\frac{hZ_0\ln(1-P_f)}{4\pi\gamma_Z\,\Phi(Z_{tot})}\right)^{1/m} R_g^{-j/m} \quad (11)$$

taking $\sigma_{nom} = \sigma_{f,nom}$ and replacing $Z_{tot}$ by $Z_{eff}$. Here $h = 1$ and $j = 2$, for surface flaws, while for volume flaws $h = j = 3$. Only in the case of surface flaws causing failure, the Hertzian failure criterion formulated in section 2.2 (equation (9)) can be directly employed by substituting the relation $\sigma_T = (1 - 2\nu_g)\sigma_0/3$ (equation (8)) for $\sigma_{f,nom}$.

## 3. Experimental Method

[19] We now report a series of diametric compression experiments performed on single sand grains aimed to test the applicability of the above micromechanical models for single-grain failure. Two series of experiments were performed:

[20] 1. Selected, single grains: These were performed on 20 selected, well-rounded grains ($d$ = 378 ± 22 $\mu$m) with measurable grain radius of curvature and aimed to calculate the flaw size at failure.

[21] 2. Randomly sampled grain size batches: These were performed for four different grain size fractions (115 ± 9 $\mu$m, 196 ± 16 $\mu$m, 275 ± 25 $\mu$m and 378 ± 22 $\mu$m) and carried out on randomly chosen, single grains from each fraction, without measuring grain surface radii of curvature. For each grain size batch, this was repeated 200 times, i.e., for 200 grains per batch. These experiments aimed to test the validity of our microcracking models (equations (9), (10), and (11)). A summary of the experimental conditions of the batch tests is shown in Table 1.

### 3.1. Starting Material

[22] We performed our experiments on sand obtained from unaltered samples taken from the Heksenberg Formation (Middle Miocene age), at the Beaujean quarry near Heerlen, The Netherlands. The sand was sieved to obtain grain size fractions of 115 ± 9 $\mu$m, 196 ± 16 $\mu$m, 275 ± 25 $\mu$m and 378 ± 22 $\mu$m. Inductively Coupled Plasma Emission Spectroscopy (ICP-ES) measurements on the sieved material indicated a quartz content of at least 99 wt %, with zircon and Na,Al-rich feldspar present as trace minerals. The feldspar trace material was successfully removed from each batch by washing in water using a gravitational separation method. Imaging of the sand, using scanning electron microscopy (SEM), showed that most sand grains are subrounded and have a pitted and grooved, but otherwise smooth surface. Some grains (<0.5 wt %) possess a thin surface layer of iron (hydr)oxide.

### 3.2. Experimental Setup and Data Acquisition

[23] One-dimensional brittle crushing tests have been performed on single sand grains loaded between flat, ceramic composite (TiC + 30 wt% $A1_2O_3$) anvils at room temperature and using a constant anvil displacement rate of ~0.1 mm/min, i.e., strain rates of approximately $4{\cdot}10^{-3}$ to $2{\cdot}10^{-2}$ $s^{-1}$. Loading was achieved using a conventional, motor-driven testing rig. The anvils were 12.65 mm in diameter by 8 mm in thickness, having a Young's modulus $E$ of 400 GPa and a Poisson's ratio $\nu$ of 0.23 [*CeramicSOURCE*, 1991].

[24] Anvil position was measured using a Hewlett Packard linear variable differential transformer (LVDT, stroke 1.27 mm) mounted directly across the sand grain sample. Therefore, no correction of the displacement measurements was needed. Load was measured with a load cell (Transducer Inc., 100 lbs force full scale). For each grain, the initial diameter ($x$), i.e., the grain height measured parallel to the loading axis, and the critical force at failure ($F_c$) were accu-

**Table 1.** Overview of the Crushing Tests Performed On Randomly Sampled Single Grains From Four Different Grain Size Batches, Under Various Test Conditions, and Using Different Types of Substrate Material[a]

| Test Conditions | Grain Size, d ($\mu$m) | | | |
|---|---|---|---|---|
| | 115 ± 9 | 196 ± 16 | 275 ± 25 | 378 ± 22 |
| Wet | Brass | Brass | Brass | Brass |
| Lab dry | Teflon | | Teflon | Teflon |
| Lab dry | | | None | |
| Lab dry | | | Brass | |
| Lab dry | | | Aluminum | |

[a]Each grain size batch consists of 200 single grains tested under the given conditions.

rately determined from a two-channel flatbed recorder displaying the load and position signals as a function of time.

[25] The anvil displacement rate was checked against a 0.01 mm resolution dial gauge and a digital stopwatch, resolving $0.1 \pm 10^{-3}$ mm/min. The LVDT was calibrated in the range ±1 mm using this dial gauge and a digital voltmeter (DVM, accuracy ±0.05%). The load cell was calibrated in the range 0–35 N with respect to a second load cell (Entran ELH-401, weight 150 lbs) using similar DVM's. The Entran load cell specifications themselves were checked against known weights, in the range 0–25 N. Conventional error analysis has shown the standard errors in $x$ and $F_c$ to be less than 0.77% and 1.16% respectively.

### 3.3. Testing Procedure

[26] The selected grain tests were carried out on well-rounded grains with measurable radius of curvature chosen from the 378 ± 22 $\mu$m sieved fraction. In preparing grains for these selected grain tests, a single layer of sand grains was first immersed in an epoxy resin film deposited on a glass slide. After hardening of the resin, a quarter to a third of the average grain height was removed by gentle polishing, after which the epoxy resin was dissolved in ethanol. From this sample of grains, individual grains were selected using light microscopy, on the basis of a visibly spherical or ellipsoidal smooth surface opposite to the polished flat. The selected grains were subsequently photographed in perpendicular directions corresponding to the maximum and minimum radii of curvature, $R'_g$ and $R''_g$ respectively. These radii were determined, with an estimated 10% relative error, from photographic prints by fitting circles to the grain surface profile. Brittle crushing tests were performed on the selected grains with the polished flat placed downward on a 50 $\mu$m brass foil and with the grains immersed in a drop of distilled water, i.e., under wet conditions. The soft substrate was used to eliminate tensile stresses arising from grain surface irregularities, in order to prevent cracks from initiating at the flat base of the grain.

[27] The batch tests were carried out on randomly sampled batches of 200 grains, taken from each of the four grain size fractions with no attempt to measure grain surface radii of curvature directly. In the experiments, each of the grains was placed on a 50–60 $\mu$m thick foil of soft substrate (see Figure 1), after which the critical force at failure would be measured. For "lab dry" experiments the substrate, when used, consisted of Teflon, brass, or aluminum foil, while under wet conditions only brass foil was used as a substrate (see Table 1). It should be noted that the measured critical force at failure did not depend significantly on the type of substrate. As most results were obtained for either brass or Teflon substrate, we will continue to present those results.

## 4. Mechanical Data

### 4.1. Selected Single Grain Data

[28] We plotted the critical force at failure ($F_c$) data, obtained from the crushing tests performed on the selected single grains, as a function of the equivalent radius of curvature $R_e$, as shown in Figure 2. The equivalent radius of curvature is defined as $R_e = \sqrt{(R'_g R''_g)}$, where $R'_g$ and $R''_g$ are the maximum and minimum radii of curvature, respectively (cf. Section 3.3). The data show a broad scatter and the clear trend, expected if the material would follow either Hertzian theory (slope of 2) or the model by *Zhang et al.* [1990], assuming a linear relation between flaw size and grain size (slope of 0.5), is not visible for our data. The poor repeatability of the experiments inhibits us to make any inferences on a correlation between the critical force at failure and mean grain size.

### 4.2. Randomly Sampled Single Grain Batch Data

[29] Overall, for all batches tested, the $F_c$ data roughly follow a lognormal distribution and the initial grain diameter ($x$) data a normal distribution. This enables arithmetic averages (means) and sample standard deviations of $\ln F_c$ and $x$ to be calculated employing the lognormal and normal distribution models respectively. The means of the critical force at failure distributions obtained from crushing experiments on the various batches tested are shown as a function of grain size in Figure 3 (Teflon substrate, "lab dry"; brass substrate, wet). Grain size is plotted either in terms of the mean measured initial grain diameter $x$, or as the equivalent sphere mean grain size. The latter is obtained by fitting a sphere to the mean grain volume of the sand grains sampled from each grain size batch, the mean grain volume being calculated from the sample mass, the number of constituent grains and the density of quartz. Overall, there can be seen very little difference in slope between the measured and equivalent sphere data for both dry and wet conditions. In addition, there is only a limited amount of data available and a relatively big error in mean grain size, which makes the significance of any differences between the two data sets questionable. However, taking the available data we cannot eliminate any influence of humidity or substrate type on the critical force at failure. The data show that $F_c$ can be considered proportional to $d^{1.3}$.

## 5. Discussion

[30] We measured the critical force at failure for selected grains (378 ± 22 $\mu$m) and grain size batches (115 ± 9 $\mu$m, 196 ± 16 $\mu$m, 275 ± 25 $\mu$m and 378 ± 22 $\mu$m). Now we will use the data obtained in our selected grain experiments to calculate the flaw size at failure. In addition, we will apply our statistical model for single-grain failure (equations (9)–(11)) to our batch data to test the validity of the micromechanical model.

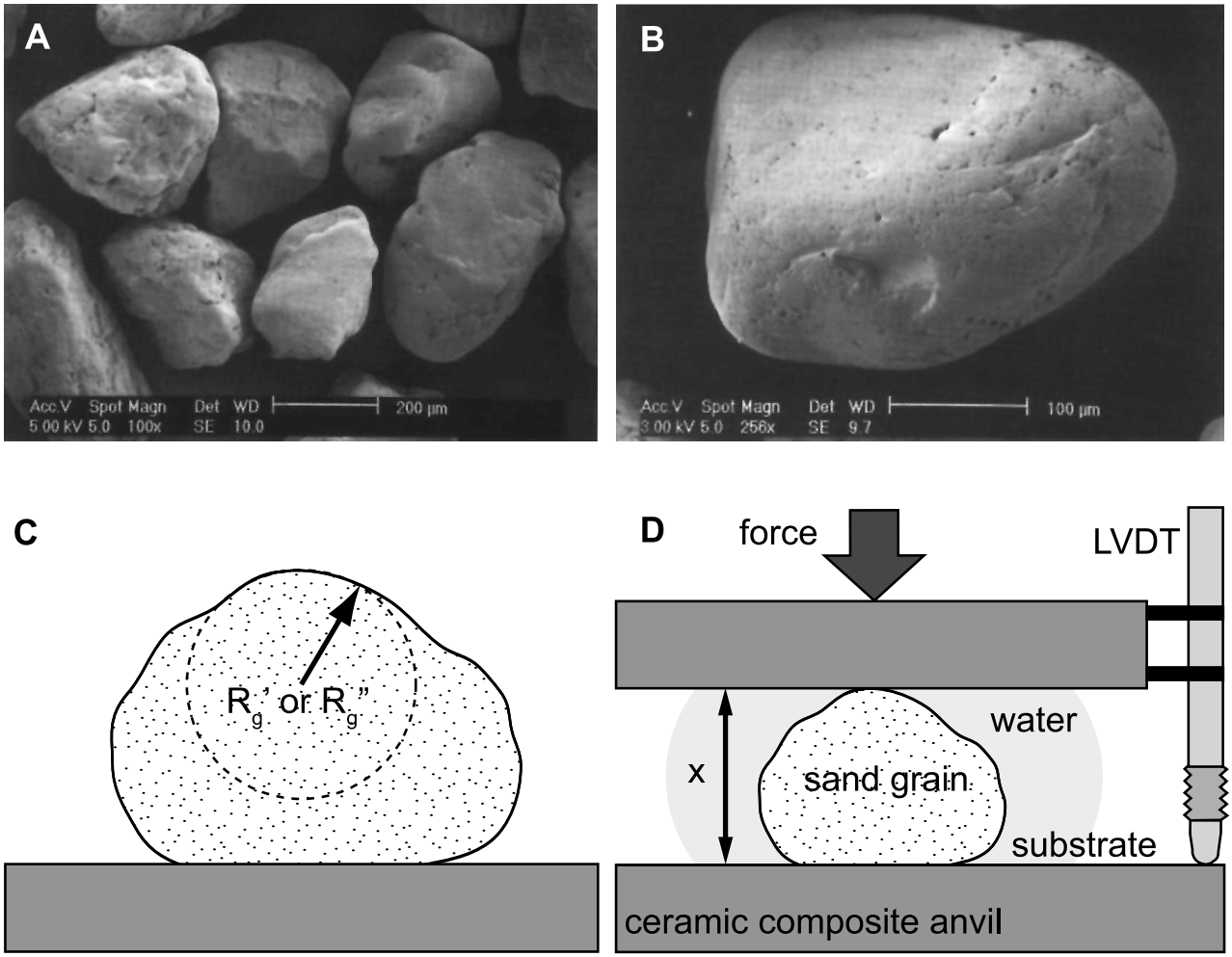


**Figure 1.** (a) SEM micrograph of the starting material used in the experiments (shown grain size fraction, $d = 275 \pm 25$ $\mu$m); (b) close-up of one of the grains showing that most sand grains appear as subrounded and show a generally smooth surface with patches of pits, grooves/scratches and depressions created by broken out pieces; (c) cartoon illustrating the measurement of the minimum and maximum radii of curvature, depending on grain orientation; (d) schematic diagram showing the anvil loading configuration used in the crushing tests on single sand grains.

### 5.1. Critical Flaw Dimension at Failure

[31] As the selected grains possessed smooth spherical or ellipsoidal contact surfaces (cf. Section 3.3), the force at failure data (see Figure 2) can be converted to the nominal failure stress $\sigma_{f,nom}$, applying the Hertzian failure criterion (see section 2.2, equation (8), i.e., taking $\sigma_{f,nom} = \sigma_T$) and assuming that the Young's modulus and Poisson's ratio of quartz are equal to 95.68 GPa and 0.077, respectively [*Simmons and Wang*, 1971; *Sumino and Anderson*, 1984]. This calculation shows that the nominal failure stress for sand grains (378 ± 22 $\mu$m) was of the order of several GPa.

[32] In addition, it is possible to apply the Hertzian micromechanical model (equations (9) and (10)) to estimate the size of the flaws causing failure of individual grains ($c_f$). The fracture toughness ($K_{Ic}$) of quartz was considered to be 1 MN $m^{-3/2}$, a representative value based on double torsion tests performed on synthetic quartz single crystals at room temperature and under ambient dry or wet conditions [*Atkinson*, 1979; *Atkinson and Meredith*, 1987]. The critical flaw dimension at failure values thus obtained are plotted as a function of the equivalent radius of curvature $R_e$ (Figure 4). For the grains with spherical surfaces, the data show an average $c_f$ of 0.115 $\mu$m, while for the ellipsoidal grains $c_f$ is approximately 0.057 $\mu$m. With the exception of the three topmost data points, the data show a relatively positive trend between grain size and critical flaw size. It is possible that the three grains that appear to be off trend had larger pretest flaws, due to preparation-induced damage.

[33] In the literature, various estimates of the Griffith flaw dimension have been reported. *Zhang et al.* [1990] compiled critical effective pressure data ($P_{cr}$) for porous quartzitic rocks and granular quartz sand of varying grain size and porosity. At the critical pressure, accelerated porosity decrease was observed during loading. Assuming the compaction behavior to be time independent, this point is believed to be the onset of major grain crushing. On the basis of an aggregate compac-

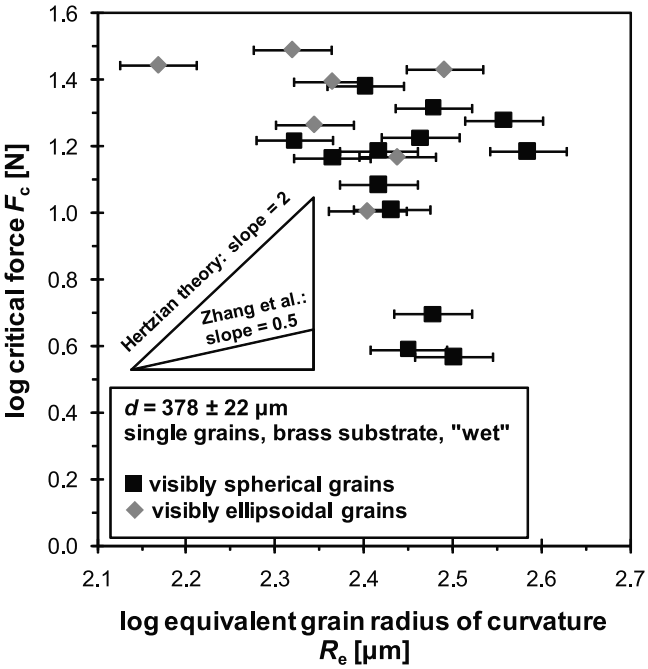


**Figure 2.** Log critical force at failure $F_c$ versus log equivalent grain radius of curvature $R_e$ for the data obtained in the selected grain tests (378 ± 22 $\mu$m, brass substrate, wet). The data have been subdivided in grains with visibly spherical (squares) or ellipsoidal (diamonds) contact surfaces. Note that there is no visible trend.

tion model adopting the same failure criterion as described by our equation (9), *Zhang et al.* [1990] used the $P_{cr}$ data to evaluate the flaw sizes at failure ($c_f$). For Ottawa sand ($d$ = 75–1000 $\mu$m), they obtained critical $c_f$ values in the range 0.0135 ± 0.0015 $\mu$m using a $K_{Ic}$ equal to 0.307 MN m$^{-3/2}$ [cf. *Atkinson and Avdis*, 1980]. However, *Ferguson et al.* [1987] report this $K_{Ic}$ value to be miscalculated; instead they recalculated a value of 1.3 MN m$^{-3/2}$. Reinterpreting the $P_{cr}$ data for Ottawa sand using $K_{Ic}$ = 1 MN m$^{-3/2}$ yields flaw sizes at failure in the range 0.14 ± 0.02 $\mu$m, which is within the same range as the flaw dimension at failure presented in this study for spherical surfaces (0.115 $\mu$m). However, it is important to note that the flaw dimension associated with failure is not necessarily equal to the initial flaw dimension ($c_0$). During continued loading, an initial flaw may extend either, at a stress intensity $K_I < K_{Ic}$, by subcritical crack growth or, at the critical point $K_I = K_{Ic}$, in a stable or equilibrium manner if $dK_I/dc < 0$. Only if the instability criterion $dK_I/dc > 0$ is satisfied at the critical point, unstable flaw propagation will occur leading to catastrophic failure [*Mat and Lawn*, 1986]. This means that the critical flaw sizes determined from our experiments can be considered a lower boundary, as our tests were most likely too rapid for subcritical crack growth to have played a role.

[34] In the above, we used Hertzian contact theory to calculate the maximum tensile stress at the edge of the contact causing failure, assuming grain failure initiated there. However, as shown by *Hiramatsu and Oka* [1966], a sphere under a uniformly distributed, diametric load attains a maximum tensile stress at the edge of the contact area, which then trails off toward a lower tensile stress, and eventually a compressive stress, away from the contact area. This means that (smaller) tensile stresses also exist just outside of the contact area. As a result, a (big) flaw outside of the contact area may also cause grain failure, though at (local) tensile stresses lower than those acting on the contact edge. Stress distribution analyses have already shown this to be a possibility [*Hiramatsu and Oka*, 1966; *Shipway and Hutchings*, 1993]. If this was the case in our experiments then the stresses calculated from the failure criterion overestimate the strength of the material, leading to estimated critical flaw sizes that are too small. Given the high nominal stress at failure values that were obtained in our tests (i.e., several GPa), it is not unlikely that failure occurred along flaws existing outside the contact area. Now, taking the equations proposed by *Hiramatsu and Oka* [1966] and assuming that $\nu = 0.25$, it can be seen that for an angular cap of 5.7°, i.e., a/R = 0.1 [see also *Brzesowsky*, 1995, chap. 2], the tensile stresses outside the contact area $\sigma_{f,nom}$ roughly show a linear relation with angular distance $\theta$ from the center of the contact. For values of $\theta$ up to 20°, this leads to $\alpha\sigma_{f,nom}$, where $\alpha$ is a linear scaling factor. Hence, the measured force at failure is related to the critical flaw size as $F_c \propto 1/(\alpha^3 c_f \sqrt{c_f})$. If the actual tensile stress at failure was only half (i.e., near field of the contact area, $\alpha$ = 1/2) to one-tenth (i.e., far field of the contact area, $\alpha$ = 0.1) of the calculated stress at failure $\sigma_{f,nom}$ [see, e.g., *Brzesowsky*,

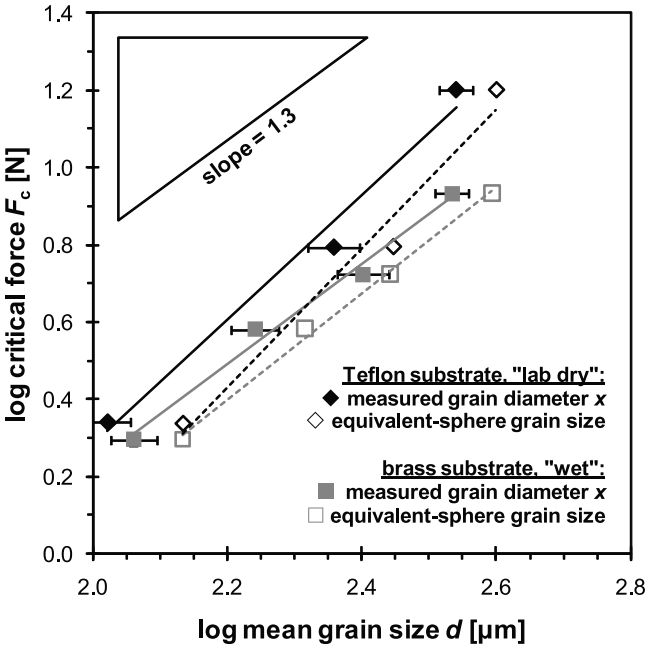


**Figure 3.** Log critical force $F_c$ versus log mean grain size $d$ plot showing the effect of grain size and experimental conditions on the critical force at failure. As can be seen, the experimental conditions do not appear to strongly affect the dependence of $F_c$ on $d$, i.e., the slope of the curves. However, it should also be noted that there is only a limited amount of data available. Equivalent sphere grain size is obtained by fitting a sphere to the mean grain volume of the grains from each batch, which in turn is determined from the sample mass, number of grains and the density of quartz.

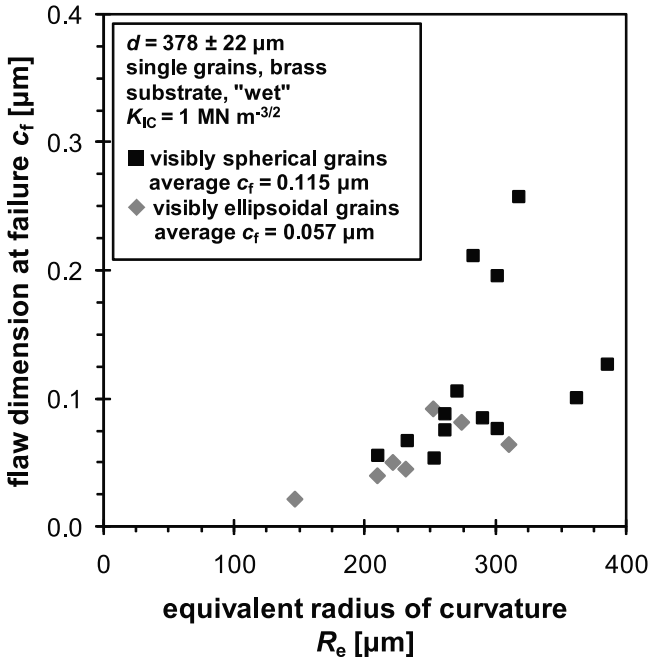


**Figure 4.** Flaw dimension at failure $c_f$ versus equivalent grain radius of curvature $R_e$ obtained by translating critical force at failure data for visibly spherical and ellipsoidal grain contact surfaces (378 ± 22 $\mu$m, brass substrate, wet; see Figure 3), using the Hertzian/LEFM model (equations (9) and (10)).

1995; *Kienzler and Schmitt*, 1990], the calculated critical flaw size will be 1 to 3 orders of magnitude bigger (i.e., ~1–100 $\mu$m). It should be noted that these values are in accordance with the flaws observed on the surfaces of the sand grains used in this study, which show pits (~5–15 $\mu$m), grooves or scratches (~5 by 50 $\mu$m), and depressions created by broken out fragments (~50 $\mu$m). Therefore, though there may have been smaller flaws present on the quartz grain surfaces, it is not unlikely that the larger surface defect caused grain failure in our experiments.

### 5.2. Applicability of the Weibull Weakest Link Model

[35] From our tests on the batch samples, we obtained a power law dependence of force at failure on grain size, with an exponent of ~1.3 (see Figure 3). Other studies show dependencies on the order of 1.1 to 2.0, for materials varying from zeolites [*Antonyuk et al.*, 2005], limestone particles [*McDowell and Amon*, 2000], sand grains [*Gallagher*, 1976], and glass spheres [*Brajer et al.*, 2003; *Kschinka et al.*, 1986], to cement and plaster spheres [*Chau et al.*, 2000; *Tsoungui et al.*, 1999; *Vallet and Charmet*, 1995; *Wu et al.*, 2004]. A typical histogram of the nominal stress at failure $\sigma_{f,nom}$, obtained from translating the $F_c$ data for a batch of single grains ($d$ = 275 ± 25 $\mu$m, brass substrate, wet) using the Hertzian failure criterion and assuming spherical grains, is shown in Figure 5. The mean nominal stress at failure for this batch of grains is approximately 2 GPa.

[36] Studies on glass spheres [*Kschinka et al.*, 1986], sand grains [*Gallagher*, 1976] and limestone particles [*McDowell and Amon*, 2000], among others, showed a clear dependence of failure stress on grain size, in terms of the Weibull weakest link model (equation (6)), given as

$$\ln\left[\ln(1-P_f)^{-1}\right] = -m\ln k + m\ln\sigma_{f,nom} \qquad (12)$$

The estimator for $(P_f)_j$ denotes $(P_f)_j = (j - 0.5)/n$, where $n$ is the total number of samples tested and $j$ is the rank of the sample in order of increasing $(\sigma_f)_j$ [*Dortmans and With*, 1991]. Figure 6 shows converted $\sigma_{f,nom}$ data obtained from the crushing tests on different grain size sand batches (brass substrate, wet). Linear, least squares regression of the $\sigma_{f,nom}$ data from each separate batch indicate that the Weibull parameters $m$ (i.e., from the slope) for each sand batch is approximately 6. In addition, the scale parameter $k$ decreases with increasing grain size $d$ (see Figure 6).

[37] In order to test the applicability of the Weibull weakest link model for grain failure developed in section 2.1, the grain size dependence of the $\sigma_{f,nom}$ data for each batch will be considered, employing equation (11) for the mean nominal stress at failure, defined as $\overline{\sigma}_{f,nom} = k\Gamma\left(\frac{1}{m}+1\right)!$, and the median nominal stress at failure, given as $\breve{\sigma}_{f,nom} = k\,(\ln 2)^{1/m}$. If the flaws causing grain failure in the different batches originate from a single population, the Weibull moduli $m$ obtained for each batch would have to be similar to the modulus obtained for the entire sample of grains. Surface flaws of sand grains are known to be generated due to grain collision and abrasion during sedimentary transport. Therefore, a single surface flaw population is believed to be a reasonable assumption for sand grains sampled from the same sedimentary environment with an identical transport history. This is supported by the observation that $F_c$ has a lognormal distribution for all grain size batches (see

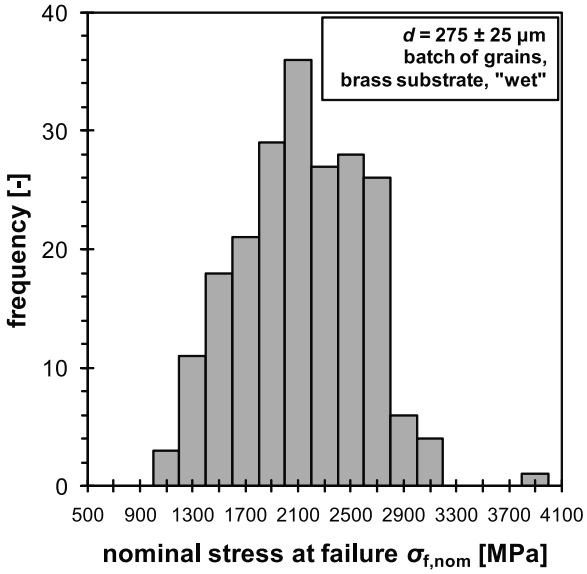


**Figure 5.** Histogram of failure stress data obtained by translating critical force at failure $F_c$ data, using the Hertzian failure criterion. Measurements were taken during experiments on a batch of 200 single grains ($d$ = 275 ± 25 $\mu$m). The mean critical stress at failure is approximately 2102 MPa (standard deviation = 463.3 MPa).

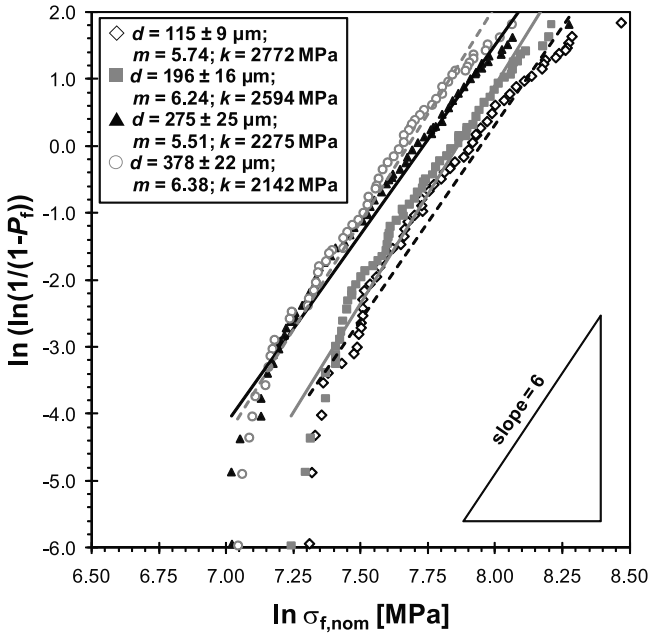


**Figure 6.** Typical Weibull plot of failure stress data versus cumulative failure probability ($P_f$) calculated using the critical force at failure data ($F_c$) and adopting the Hertzian failure criterion, assuming spherical grains. The force data have been obtained from crushing tests on the four sand grain size batches (brass substrate, wet). Best fit estimates yield a Weibull parameter $m$ of approximately 6.

Section 4.2). In case of surface flaws causing failure, the slope of lines fitting the tensile strength data should be equal to $-2/m$, according to equation (11) (with $R_g = R$), yielding $m \approx 8$ for the entire sample of grains. This value is slightly off from the moduli $m$ obtained for the separate batches of grains (see Figures 6 and 7). It is inferred that the Weibull weakest link-based model developed is not able to account for the observed grain size dependence of the grain failure stress. The case of volume flaws causing failure is not considered since the Hertzian failure criterion employed in the calculation of the strength applies only to failure arising from surface flaws.

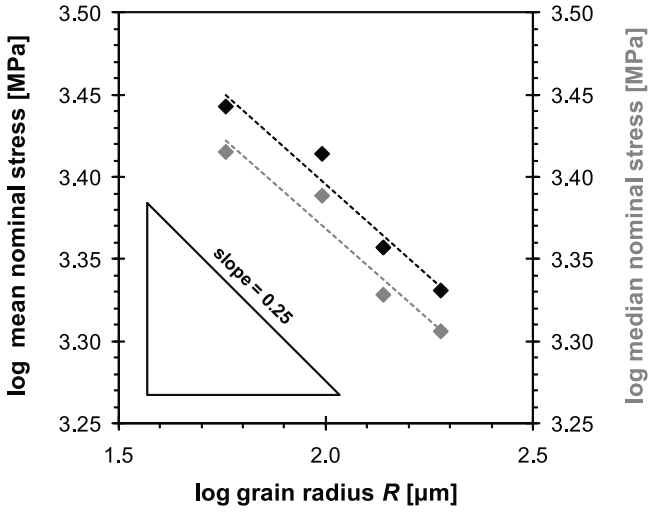


**Figure 7.** Log mean and median nominal stress at failure versus mean grain radius for the data obtained in the wet crushing tests on sand grain batches (brass substrate). In case of surface flaws causing failure, this resembles a Weibull parameter $m \approx 8$ for the entire sample of grains, notably unequal to the parameter $m$ obtained for each size batch (see Figure 6).

### 5.3. Applicability of the Hertzian/LEFM Model

[38] The grain size ($d$) dependence of the critical load at failure ($F_c$) as deduced from Figure 3 differs from that predicted by the Hertzian/LEFM model, which predicts $F_c \propto d^2$. For values of the Weibull modulus of 6 to 8 obtained in this study, a theoretical fracture model based on Weibull theory, as proposed by *Tsoungui et al.* [1999], predicts grain size power law dependencies of $F_c$ with exponents of 1–1.2 for surface flaws and 1.5–1.6 for volume flaws. The former are in accordance with our measurements on single sand grains of different grain size. The (extent of the) discrepancy between the expected and the measured grain size dependencies is attributed to the internal microstructure of the grains [*Tsoungui et al.*, 1999], such as intraparticle porosity [*McDowell and Bolton*, 1998] and flaw distribution, as this is reflected in the Weibull modulus $m$.

[39] If the basic Hertzian/LEFM assumptions of our model are correct, this implies that either the flaw dimension at failure or the effective grain contact or asperity radius must be functionally related to grain size $d = 2R_g$. To examine this possibility, the force at failure distribution data represented in Figure 3 have been converted into distributions of (1) flaw size at failure ($c_f$) assuming a perfectly spherical grain geometry and using equation (4) with $x = d = 2R_g$, and (2) into distributions of "effective" grain radii of curvature ($r_g$), characterizing asperity amplitude. In the latter case, the model is applied dropping the assumption of spherical grains, using the relation $R_g = r_g$ in equation (4)

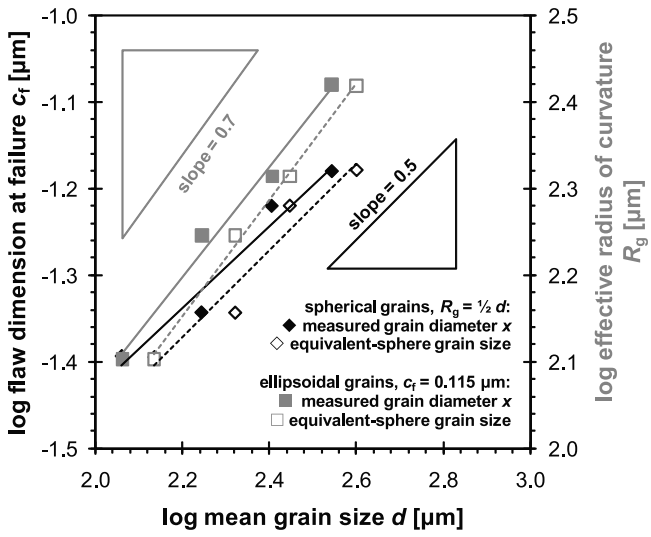


**Figure 8.** Log mean flaw dimension at failure $c_f$ versus log mean grain size $d$ obtained from the critical force at failure data of Figure 3, using the Hertzian/LEFM model, assuming spherical grains with a radius of curvature $R_g$ equal to half the measured, initial grain size.

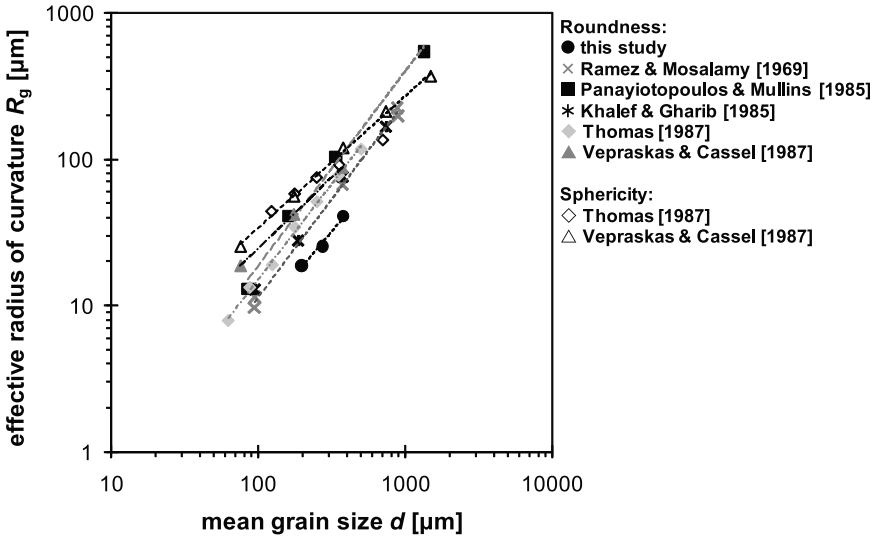


**Figure 9.** Log effective radius of curvature $r_g$ versus log grain size $d$ constructed by translating sphericity and roundness data from morphological studies on aeolian sands, plus roundness data from grain size fractions used in this study (circles).

and assuming constant $c_f$ (taken equal to the mean or lower bound value obtained from the selected grain tests).

[40] For all batches tested, however, the distributed $c_f$ values approximately follow a lognormal distribution and the $r_g$ values a normal distribution. This enables arithmetic averages (means) and sample standard deviations of ($\ln c_f$) and $r_g$ to be calculated employing the appropriate distribution models. The means of the $c_f$ and $r_g$ distributions obtained from the $F_c$ data of the size fractions represented in Figure 3 are plotted as a function of grain size ($d$) in Figure 8. The grain size plotted is either the mean measured initial grain diameter ($x$) or the equivalent sphere grain size calculated from the average grain mass. These plots show that both $c_f$ and $r_g$ can be described by a power law dependence on grain size, i.e., $c_f$ and $r_g \propto d^{0.5–0.7}$. A similar relation is obtained if the lower bound estimate for $c_f$ is used (i.e., $c_f = 0.057$ $\mu$m). If the force at failure data depicted in Figure 3 (Teflon substrate, lab dry) is likewise treated, similar results are obtained with $d^{0.45–0.7}$.

[41] In order to decide if there is any physical basis for expecting $c_f$ or $r_g$ to be related to $d$ in the manner described above, grain microstructural constraints will now be examined. First, the sand grains used in this study are not spherical whereas perfectly spherical grain geometry is assumed for computing $c_f$ from $F_c$. Moreover, if the flaws at the surface of the sand grains are assumed to be generated due to grain collision and abrasion during sedimentary transport, there is no physical basis to argue that their initial dimension ($c_0$), or the mean of their size distribution, should be grain size dependent. In addition, the selected grains with visibly spherical or ellipsoidal contact surfaces do not show a systematic relation between flaw size at failure ($c_f$) and grain size (see section 5.1). This is in accordance with observations for Yuen Long Marble made by *Wong et al.* [1996], which showed that initial crack sizes are roughly equal to the grain size for small grains (<50 $\mu$m), while $c_0$ was roughly five times smaller than the grains at larger grain sizes (>300 $\mu$m), suggesting no dependence of $c_f$ on $d$. Furthermore, *Hatzor and Palchik* [1997] stated that, on the basis of their model for initial flaw size, the assumption that initial flaw size scales with grain size is only valid in the case of low porosity–low grain size rocks. These arguments (coupled with the assumption that $c_f = c_0$) suggest that the observed grain failure behavior cannot be explained by a Hertzian/LEFM model in combination with a grain size dependent flaw size ($c_f$).

[42] Second, it is important to consider that in sedimentary petrology the shape or external morphology of quartz sand grains is characterized by independent properties of form, roundness and surface texture distinguishable by their different scales with respect to grain size [*Barrett*, 1980]. Form can be estimated by elongation parameters based on ratios involving orthogonal principal axes ($a_e > b_e > c_e$) of assumed ellipsoidal grains. It may also be quantified in terms of sphericity, defined as $d/a_e$ [*Wadell*, 1932, 1935], $(b_e c_e/a_e^2)^{1/3}$ [*Krumbein*, 1941], $(c_e^2/a_e b_e)^{1/3}$ [*Folk*, 1955; *Sneed and Folk*, 1958] or $\sqrt{(R_{ins}/R_{ci})}$ [*Riley*, 1941] where $R_{ins}$ is the radius of the largest inscribed sphere and $R_{ci}$ is the radius of the smallest circumscribed sphere. Roundness reflects grain angularity or surface roughness caused by variations in radii of curvature of edges, corners and faces. It may be quantified as $(\Sigma(r_i/R_{in}))/n$ [*Wadell*, 1932] or $r_s/R_{in}$ [*Dobkins and Folk*, 1970; *Folk*, 1978], where $r_i$ is the radius of curvature of the $i$th grain corner (of a total $n$) and $r_s$ is the radius of curvature of the sharpest corner [*Barrett*, 1980]. Sphericity and roundness defined as above can be quantified in the context of the present investigation using a simple geometric model implying the following relations

$$r_g \approx R_{ci} - R_{ins} \approx \left(\sum_{i=1}^{n} r_i\right)/n \approx r_s$$
$$a_e \approx 2R_{ci} \text{ and } c_e \approx b_e \approx 2R_{ins} \quad (13)$$
$$\text{with } d \approx 2R_{ins}$$

Figure 9 shows sphericity and roundness data compiled from morphology studies on dune sands of various grain size ($d$) converted into $r_g$ versus $d$ plots. Furthermore, roundness

($r_s/R_{in}$) has been determined in thin section of a random sample of grains from three out of four grain size fractions used in this study. The average roundness values obtained for each fraction are likewise converted into $r_g$ versus $d$ data using the relations given in equation (3) and added to Figure 9 (circles). The data depicted in this graph show $r_g$ to be approximately proportional to $d^{0.65–1.3}$. This kind of relationship is well known in sedimentary petrology and has been attributed to more effective abrasion of larger sized particles [*Donaldson et al.*, 1995]. Notably, this relation is in reasonable agreement with the $r_g$ versus $d$ plot of Figure 8. On this basis, it is inferred that the grain failure behavior observed in our batch tests is best explained by a Hertzian/LEFM model in combination with grain size dependent sphericity/roundness as expressed by the effective radius of curvature ($r_g$).

[43] In the context of the compaction of high-porosity sandstones and sands, our results imply that grain angularity may also play a role in grain failure behavior. This suggests that for granular aggregates, in addition to factors such as average grain size and porosity [*Karner et al.*, 2005; *Zhang et al.*, 1990], the radius of curvature of the grains will affect compaction behavior. Hence, more compaction is expected in rapidly subsiding basins, which contain less well-rounded grains, due to the high energy depositional environment, and depleting hydrocarbon reservoirs with more angular, coarser-grained material.

## 6. Conclusions

[44] Crushing tests have been carried out on selected, well-rounded single sand grains and on grains sampled from different grain size batches. We used the force at failure data obtained in our experiments to calculate the flaw size at failure (selected grain tests) and to validate the micromechanical models we derived, aimed to explain the observed grain size dependence of force of failure (batch tests). Our main findings can be summarized as:

[45] 1. The grain failure load ($F_c$) data obtained for the selected grains have been converted into an estimate of the size of surface flaws at failure ($c_f$) using Hertzian contact theory. The estimated flaw sizes were on the order of 0.057–0.115 $\mu$m. Taking into account failure along bigger flaws outside of the contact area resulted in flaw sizes 1 to 3 orders of magnitude bigger, which is in better accordance with the damage features observed on the sand grain surfaces.

[46] 2. We observed a grain size dependence of the force at failure of the form: $F_c \propto d^{1.3}$. In addition, the distributed force at failure data obtained for the different batches have been converted into distributions of failure stress ($\sigma_{f,nom}$). This resulted in a power law dependence of $\sigma_{f,nom}$ on grain size, i.e., $\sigma_{f,nom} \propto d^{-0.25}$. Assuming a single flaw population causing grain failure and spherical grains, a Weibull weakest link-based model for grain failure is unable to account for the observed grain size dependence of $\sigma_{f,nom}$.

[47] 3. The Hertzian/LEFM model enables the translation of the distributed $F_c$ data into distributions of $c_f$ or effective (asperity) radius of curvature ($r_g$). The data imply a power law dependence of $c_f$ or $r_g$ on grain size, i.e., $c_f$ or $r_g \propto d^{0.5–0.7}$. Since there is no clear physical basis for a grain size dependence of $c_f$ and since sphericity and roundness data for dune sands exhibit a similar relation between $r_g$ and $d$, it is inferred that a Hertzian/LEFM model assuming nonspherical grains with a distributed $r_g$, caused by surface asperities, is the most physically reasonable model for grain failure. In other words, grain failure is inferred to be controlled by propagation of surface cracks at loaded asperities under the action of the Hertzian contact stresses, which take a maximum value at the contact periphery.

[48] 4. This work provides insight into grain failure and could, therefore, shed light on the micromechanics of sand compaction used in modeling studies of both upper crustal deformation and the compaction of clastic hydrocarbon reservoirs in the (post) production phase.

## Notation

$A_{tot}$ total solid surface area.
$A_0$ elementary solid surface area.
$a$ radius of contact circle between a grain (g) and a flat plate (p).
$a_e$ orthogonal principal axes of an ellipsoidal grain, where $a_e > b_e > c_e$.
$b_e$
$c_e$
$c$ flaw dimension.
$c_0$ initial flaw dimension.
$c_f$ flaw dimension at failure.
$d$ mean grain size.
$E$ Young's modulus.
$E^*$ $E^* = \frac{(1-\nu_g)}{E_g} + \frac{(1-\nu_p)}{E_p}$.
$F$ total normal load transmitted between grain and platen.
$F_c$ critical force at failure.
$k$ Weibull scale parameter.
$K_I$ stress intensity factor.
$K_{Ic}$ fracture toughness.
$K_{eq}$ equivalent stress intensity factor.
$K_{c,eq}$ critical equivalent stress intensity factor.
$m$ Weibull modulus.
$P_{cr}$ critical effective pressure.
$P_f$ failure probability.
$q_e$ $q_e = 1 - (R''_g/R'_g)^{4/3}$.
$R$ radius of curvature.
$R_e$ equivalent radius of curvature; $R_e = \sqrt{R'_g R''_g}$.
$R_g$ grain radius of curvature.
$R'_g$ principal maximum radius of curvature.
$R''_g$ principal minimum radius of curvature.
$R_p$ (infinite) radius of curvature of a flat platen.
$R_r$ relative radius of curvature; $\frac{1}{R_r} = \frac{1}{R_g} + \frac{1}{R_p}$.
$R_{ci}$ radius of the smallest circumscribed sphere around a given grain.
$R_{ins}$ radius of the largest inscribed sphere within a given grain.
$r_g$ radius of curvature of grain asperity.
$r_i$ radius of curvature of the $i$th grain corner.
$r_s$ radius of curvature of the sharpest corner.
$V_0$ elementary solid volume.
$V_{tot}$ total solid volume.
$x$ grain diameter.
$Y$ dimensionless factor, $Y \approx 1.12$ for a single-ended edge crack.

$Z_0$ general measure for elementary solid volume or surface area.
$Z_{tot}$ general measure for total solid volume or surface area.
$\alpha$ linear scaling factor.
$\Gamma(1/m + 1)!$ gamma function for $(1/m + 1)$.
$\gamma$ scaling factor.
$\nu$ Poisson's ratio.
$\sigma_0$ normal stress at the center of the contact area.
$\sigma_{ch}$ characteristic strength.
$\sigma_{eq}$ applied equivalent stress.
$\sigma_{nom}$ nominal stress, or maximum stress in the structure.
$\sigma_{f,nom}$ nominal stress at failure, or maximum stress at failure.
$\overline{\sigma}_{f,\ nom}$ mean nominal stress at failure.
$\breve{\sigma}_{f,nom}$ median nominal stress at failure.
$\sigma_{rr}$ Hertzian radial stress.
$\sigma_T$ maximum tensile stress at the edge of the Hertzian contact.
$\Phi_{Ztot}$ dimensionless stress integral, depending on the applied equivalent stress.
$\varphi$ porosity.

## References


Antonellini, M. A., A. Aydin, and D. D. Pollard (1994), Microstructure of deformation bands in porous sandstones at Arches National Park, Utah, *J. Struct. Geol.*, *16*(7), 941–959, doi:10.1016/0191-8141(94)90077-9.

Antonyuk, S., J. Tomas, S. Heinrich, and L. Mörl (2005), Breakage behaviour of spherical granulates by compression, *Chem. Eng. Sci.*, *60*(14), 4031–4044, doi:10.1016/j.ces.2005.02.038.

Atkinson, B. K. (1979), A fracture mechanics study of subcritical tensile cracking of quartz in wet environments, *Pure Appl. Geophys.*, *117*, 1011–1024, doi:10.1007/BF00876082.

Atkinson, B. K., and V. Avdis (1980), Fracture mechanics parameters of some rock-forming minerals determined using an indentation technique, *Int. J. Rock Mech. Min. Sci. Geomech. Abstr.*, *17*(6), 383–386, doi:10.1016/0148-9062(80)90523-9.

Atkinson, B. K., and P. G. Meredith (1987), Experimental fracture mechanics data for rocks and minerals, in *Fracture Mechanics of Rock*, edited by B. K. Atkinson, pp. 477–525, Academic, London.

Barrett, P. J. (1980), The shape of rock particles, a critical review, *Sedimentology*, *27*(3), 291–303, doi:10.1111/j.1365-3091.1980.tb01179.x.

Batdorf, S. B., and J. G. Crose (1974), A statistical theory for the fracture of brittle structures subjected to nonuniform polyaxial stresses, *J. Appl. Mech.*, *41*(2), 459–464, doi:10.1115/1.3423310.

Batdorf, S. B., and H. L. Heinisch (1978), Weakest link theory reformulated for arbitrary fracture criterion, *J. Am. Ceram. Soc.*, *61*(7–8), 355–358, doi:10.1111/j.1151-2916.1978.tb09327.x.

Bazant, Z. P., Y. Xi, and S. G. Reid (1991), Statistical size effect in quasi-brittle structures: I. Is Weibull theory applicable?, *J. Eng. Mech.*, *117*(11), 2609–2622, doi:10.1061/(ASCE)0733-9399(1991)117:11(2609).

Bernabe, Y., and W. F. Brace (1990), Deformation and fracture of Berea sandstone, in *The Brittle-Ductile Transition in Rocks: The Heard Volume*, *Geophys. Monogr. Ser.*, vol. 56, edited by A. G. Duba et al., pp. 91–102, AGU, Washington, D. C.

Borg, I., M. Friedman, J. Handin, and D. V. Higgs (1960), Experimental deformation of St. Peter sand: A study of cataclastic flow, in *Rock Deformation, A Symposium*, edited by D. Griggs and J. Handin, pp. 133–191, Geol. Soc. of Am., New York.

Brajer, X., P. Forquin, R. Gy, and F. Hild (2003), The role of surface and volume defects in the fracture of glass under quasi-static and dynamic loadings, *J. Non-Cryst. Solids*, *316*(1), 42–53, doi:10.1016/S0022-3093(02)01936-1.

Brzesowsky, R. H. (1995), Micromechanics of sand failure and sand compaction, Ph.D. thesis, 180 pp., Utrecht Univ., Utrecht, Netherlands.

Burley, S. D. (1986), The development and destruction of porosity within Upper Jurassic reservoir sandstones of the Piper and Tartan fields, outer Moray Firth, North Sea, *Clay Miner.*, *21*(4), 649–694, doi:10.1180/claymin.1986.021.4.14.

CeramicSOURCE (1991), *Annual Company Directory and Buyer's Guide*, vol. 7, Am. Ceram. Soc., Westerville, Ohio.

Chao, L.-Y., and D. K. Shetty (1990), Equivalence of physically based statistical fracture theories for reliability analysis of ceramics in multiaxial loading, *J. Am. Ceram. Soc.*, *73*(7), 1917–1921, doi:10.1111/j.1151-2916.1990.tb05245.x.

Chau, K. T., X. X. Wei, R. H. C. Wong, and T. X. Yu (2000), Fragmentation of brittle spheres under static and dynamic compressions: Experiments and analyses, *Mech. Mater.*, *32*(9), 543–554, doi:10.1016/S0167-6636(00)00026-0.

Chester, J. S., S. C. Lenz, F. M. Chester, and R. A. Lang (2004), Mechanisms of compaction of quartz sand at diagenetic conditions, *Earth Planet. Sci. Lett.*, *220*, 435–451, doi:10.1016/S0012-821X(04)00054-8.

Chuhan, F. A., A. Kjeldstad, K. Bjørlykke, and K. Høeg (2002), Porosity loss in sand by grain crushing—Experimental evidence and relevance to reservoir quality, *Mar. Pet. Geol.*, *19*(1), 39–53, doi:10.1016/S0264-8172(01)00049-6.

Chuhan, F. A., A. Kjeldstad, K. Bjørlykke, and K. Høeg (2003), Experimental compression of loose sands: Relevance to porosity reduction during burial in sedimentary basins, *Can. Geotech. J.*, *40*(5), 995–1011, doi:10.1139/t03-050.

Dobkins, J. E., and R. L. Folk (1970), Shape development on Tahiti-Nui, *J. Sediment. Res.*, *40*(4), 1167–1203.

Donaldson, E. C., G. V. Chilingarian, and H. H. Rieke (1995), Stresses in sediments, in *Subsidence Due to Fluid Withdrawal*, edited by G. V. Chilingarian et al., pp. 165–192, Elsevier Sci., Amsterdam.

Doornhof, D., T. G. Kristiansen, N. B. Nagel, P. D. Patillo, and C. Sayers (2006), Compaction and subsidence, *Oilfield Rev.*, *18*(3), 50–68.

Dortmans, L. J. M. G., and G. With (1991), Noise sensitivity of fit procedures for Weibull parameter extraction, *J. Am. Ceram. Soc.*, *74*(9), 2293–2294, doi:10.1111/j.1151-2916.1991.tb08298.x.

Dunn, D. E., L. J. Lafountain, and R. E. Jackson (1973), Porosity dependence and mechanism of brittle fracture in sandstones, *J. Geophys. Res.*, *78*(14), 2403–2417, doi:10.1029/JB078i014p02403.

Ferguson, C. C., G. E. Lloyd, and R. J. Knipe (1987), Fracture mechanics and deformation processes in natural quartz: A combined Vickers indentation, SEM, and TEM study, *Can. J. Earth Sci.*, *24*, 544–555, doi:10.1139/e87-053.

Fok, S. L., and J. Smart (1993), Discriminating between fracture criteria in the prediction of failure probability of brittle materials, *Eng. Fract. Mech.*, *46*(3), 519–528, doi:10.1016/0013-7944(93)90244-M.

Folk, R. L. (1955), Student operator error in determination of roundness, sphericity, and grain size, *J. Sediment. Res.*, *25*(4), 297–301.

Folk, R. L. (1978), Angularity and silica coatings of Simpson Desert sand grains, Northern Territory, Australia, *J. Sediment. Res.*, *48*(2), 611–624.

Gallagher, J. J. (1976), Fracturing of quartz sand grains, paper presented at 17th Symposium on Rock Mechanics, Am. Rock Mech. Assoc., Snowbird, Utah.

Gallagher, J. J. (1987), Fractography of sand grains broken by uniaxial compression, in *Clastic Particles: Scanning Electron Microscopy and Shape Analysis of Sedimentary and Volcanic Clasts*, edited by J. R. Marshall, pp. 189–228, Van Nostrand Reinhold, New York.

Gallagher, J. J., M. Friedman, J. Handin, and G. M. Sowers (1974), Experimental studies relating to microfracture in sandstone, *Tectonophysics*, *21*, 203–247, doi:10.1016/0040-1951(74)90053-5.

Gill, J. J., C. Miglionico, and M. Andrews (1990), Measurement of the microstructural response of lightly cemented granular soils under uniaxial strain conditions, in *Micromechanics of Failure of Quasi-Brittle Materials*, edited by S. P. Shah et al., pp. 206–213, Elsevier Sci., New York.

Groshong, R. H. J. (1988), Low-temperature deformation mechanisms and their interpretation, *Geol. Soc. Am. Bull.*, *100*(9), 1329–1360, doi:10.1130/0016-7606(1988)100<1329:LTDMAT>2.3.CO;2.

Hangx, S. J. T., C. J. Spiers, and C. J. Peach (2010), Creep of simulated reservoir sands and coupled chemical-mechanical effects of $CO_2$ injection, *J. Geophys. Res.*, *115*, B09205, doi:10.1029/2009JB006939.

Hatzor, Y. H., and V. Palchik (1997), The influence of grain size and porosity on crack initiation stress and critical flaw length in dolomites, *Int. J. Rock Mech. Min. Sci.*, *34*(5), 805–816, doi:10.1016/S1365-1609(96)00066-6.

Hellen, T. K., and W. S. Blackburn (1975), The calculation of stress intensity factors for combined tensile and shear loading, *Int. J. Fract.*, *11*(4), 605–617, doi:10.1007/BF00116368.

Hertz, H. (1896), *Miscellaneous Papers*, 340 pp., MacMillan, London.

Hettema, M., E. Papamichos, and P. M. T. M. Schutjens (2002), Subsidence delay: Field observations and analysis, *Oil Gas Sci. Technol.*, *57*(5), 443–458, doi:10.2516/ogst:2002029.

Hiramatsu, Y., and Y. Oka (1966), Determination of the tensile strength of rock by a compression test of an irregular test piece, *Int. J. Mech. Min. Sci. Geomech. Abstr.*, *3*(2), 89–90, doi:10.1016/0148-9062(66)90002-7.

Huber, M. T. (1904), Zur Theorie der Berührung fester elastischer Körper, *Ann. Phys.*, *319*(6), 153–163, doi:10.1002/andp.19043190611.

Jayatilaka, A. D. S., and K. Trustrum (1977), Statistical approach to brittle fracture, *J. Mater. Sci.*, *12*(7), 1426–1430, doi:10.1007/BF00540858.
Johnson, K. L. (1987), *Contact Mechanics*, Cambridge Univ. Press, Cambridge, U. K.
Karner, S. L., F. M. Chester, A. K. Kronenberg, and J. S. Chester (2003), Subcritical compaction and yielding of granular quartz sand, *Tectonophysics*, *377*, 357–381, doi:10.1016/j.tecto.2003.10.006.
Karner, S. L., J. S. Chester, F. M. Chester, A. K. Kronenberg, and A. Hajash (2005), Laboratory deformation of granular quartz sand: Implications for the burial of clastic rocks, *AAPG Bull.*, *89*(5), 603–625, doi:10.1306/12200404010.
Kienzler, R., and W. Schmitt (1990), On single-particle comminution: Numerical analysis of compressed spheres, *Powder Technol.*, *61*(1), 29–38, doi:10.1016/0032-5910(90)80063-5.
Kittl, P., and G. Diaz (1988), Weibull's fracture statistics or probabilistic strength of materials: State of the art, *Res. Mech.*, *24*, 99–207.
Krumbein, W. C. (1941), Measurement and geological significance of shape and roundness of sedimentary particles, *J. Sediment. Res.*, *11*(2), 64–72.
Kschinka, B. A., S. Perrella, H. Nguyen, and R. C. Bradt (1986), Strengths of glass spheres in compression, *J. Am. Ceram. Soc.*, *69*(6), 467–472, doi:10.1111/j.1151-2916.1986.tb07447.x.
Lambe, T. W., and R. V. Whitman (1969), *Soil Mechanics*, Wiley, New York.
Lamon, J. (1988), Statistical approaches to failure for ceramic reliability assessment, *J. Am. Ceram. Soc.*, *71*(2), 106–112, doi:10.1111/j.1151-2916.1988.tb05825.x.
Lawn, B. R. (1993), *Fracture of Solids*, 2nd ed., Cambridge Univ. Press, Cambridge, U. K., doi:10.1017/CBO9780511623127.
Lee, K. L., and I. Farhoomand (1967), Compressibility and crushing of granular soil in anisotropic triaxial compression, *Can. Geotech. J.*, *4*(1), 68–86, doi:10.1139/t67-012.
Mat, Y.-W., and B. R. Lawn (1986), Crack stability and toughness characteristics in brittle materials, *Annu. Rev. Mater. Sci.*, *16*(1), 415–439, doi:10.1146/annurev.ms.16.080186.002215.
Matthews, J. R., F. A. McClintock, and W. J. Shack (1976), Statistical determination of surface flaw density in brittle materials, *J. Am. Ceram. Soc.*, *59*(7–8), 304–308, doi:10.1111/j.1151-2916.1976.tb10970.x.
McDowell, G. R. (2002), On the yielding and plastic compression of sand, *J. Jpn. Geotech. Soc. Soils Found.*, *42*(1), 139–145.
McDowell, G. R., and A. Amon (2000), The application of Weibull statistics to the fracture of soil particles, *J. Jpn. Geotech. Soc. Soils Found.*, *40*(5), 133–141.
McDowell, G. R., and M. D. Bolton (1998), On the micromechanics of crushable aggregates, *Geotechnique*, *48*(5), 667–679, doi:10.1680/geot.1998.48.5.667.
McDowell, G. R., and A. Humphreys (2002), Yielding of granular materials, *Granular Matter*, *4*(1), 1–8.
Myer, L. R., J. M. Kemeny, Z. Zheng, R. Suarez, R. T. Ewy, and N. G. W. Cook (1992), Extensile cracking in porous rock under differential compression stress, *Appl. Mech. Rev.*, *45*(8), 263–280.
Nakata, Y., A. F. L. Hyde, M. Hyodo, and H. Murata (1999), A probabilistic approach to sand particles crushing in the triaxial test, *Geotechnique*, *49*(5), 567–583, doi:10.1680/geot.1999.49.5.567.
Nakata, Y., Y. Kato, M. Hyodo, A. F. L. Hyde, and H. Murata (2001), One-dimensional compression behaviour of uniformly graded sand related to single particle crushing strength, *J. Jpn. Geotech. Soc. Soils Found.*, *41*(2), 39–51.
Quinn, G. D., and R. Morrell (1991), Design data for engineering ceramics: A review of the flexure test, *J. Am. Ceram. Soc.*, *74*(9), 2037–2066, doi:10.1111/j.1151-2916.1991.tb08259.x.
Riley, N. A. (1941), Projection sphericity, *J. Sediment. Res.*, *11*(2), 94–95.
Scholten, H. F. (1993), Evaluation of multiaxial fracture models for technical ceramics, Ph.D. thesis, Tech. Univ. Eindhoven, Eindhoven, Netherlands.
Schutjens, P. M. T. M., H. de Ruig, and J. G. van Munster (1994), Compressibility measurement and acoustic characterisation of quartz-rich consolidated reservoir rock (Brent Field, North Sea), paper presented at SPE/ISRM International Conference, Soc. of Pet. Eng., Rotterdam, Netherlands.
Shipway, P. H., and I. M. Hutchings (1993), Fracture of brittle spheres under compression and impact loading: I. Elastic stress distributions, *Philos. Mag. A*, *67*(6), 1389–1404, doi:10.1080/01418619308225362.
Simmons, G., and H. F. Wang (1971), *Single Crystal Constants and Calculated Aggregate Properties*, MIT Press, Cambridge, Mass.
Smart, J., and S. L. Fok (1994), Discriminating between volume and surface integral theories for brittle materials, *Eng. Fract. Mech.*, *48*(6), 801–810, doi:10.1016/0013-7944(94)90187-2.
Sneed, E. D., and R. L. Folk (1958), Pebbles in the lower Colorado river, Texas: A study in particle morphogenesis, *J. Geol.*, *66*, 114–150, doi:10.1086/626490.
Stanley, P., H. Fessler, and A. D. Sivill (1973), An engineer's approach to the prediction of failure probability of brittle components, *Proc. Br. Ceram. Soc.*, *22*, 453–487.
Sumino, Y., and O. L. Anderson (1984), Elastic constants of minerals, in *Handbook of Physical Properties of Rocks*, vol. III, edited by R. S. Carmichel, pp. 39–138, CRC Press, Boca Raton, Fla.
Thiemeier, T., A. Brückner-Foit, and H. Kölker (1991), Influence of the fracture criterion on the failure prediction of ceramics loaded in biaxial flexure, *J. Am. Ceram. Soc.*, *74*(1), 48–52, doi:10.1111/j.1151-2916.1991.tb07295.x.
Tsoungui, O., D. Vallet, J.-C. Charmet, and S. Roux (1999), Size effects in single grain fragmentation, *Granul. Matter*, *2*(1), 19–27, doi:10.1007/s100350050030.
Vallet, D., and J. C. Charmet (1995), Mechanical behaviour of brittle cement grains, *J. Mater. Sci.*, *30*(11), 2962–2967, doi:10.1007/BF00349670.
Vesíc, A. S., and G. W. Clough (1968), Behaviour of granular materials under high stresses, *J. Soil Mech. Found. Div. Am. Soc. Civ. Eng.*, *3*, 661–687.
Wadell, H. (1932), Volume, shape, and roundness of rock particles, *J. Geol.*, *40*, 443–451, doi:10.1086/623964.
Wadell, H. (1935), Volume, shape, and roundness of quartz particles, *J. Geol.*, *43*, 250–280, doi:10.1086/624298.
Weibull, W. (1951), A statistical distribution function of wide applicability, *J. Appl. Mech.*, *18*, 293–297.
Wilson, J. C., and E. F. McBride (1988), Compaction and porosity evolution of Pliocene sandstones, Ventura Basin, California, *AAPG Bull.*, *72*(6), 664–681.
Wissler, T. M., and G. Simmons (1985), The physical properties of a set of sandstones—Part II. Permanent and elastic strains during hydrostatic compression to 200 MPa, *Int. J. Mech. Min. Sci. Geomech. Abstr.*, *22*(6), 393–406, doi:10.1016/0148-9062(85)90004-X.
Wong, R. H. C., K. T. Chau, and P. Wang (1996), Microcracking and grain size effect in Yuen Long marbles, *Int. J. Mech. Min. Sci. Geomech. Abstr.*, *33*(5), 479–485, doi:10.1016/0148-9062(96)00007-1.
Wong, T.-F. (1990), Mechanical compaction and the brittle-ductile transition in porous sandstones, *Geol. Soc. Spec. Publ.*, *54*, 111–122.
Wong, T.-F., and P. Baud (1999), Mechanical compaction of porous sandstone, *Oil Gas Sci. Technol.*, *54*(6), 715–727, doi:10.2516/ogst:1999061.
Wong, T.-F., C. David, and W. Zhu (1997), The transition from brittle faulting to cataclastic flow on porous sandstones: Mechanical deformation, *J. Geophys. Res.*, *102*(B2), 3009–3025, doi:10.1029/96JB03281.
Wu, S., and R. H. Groshong (1991), Low-temperature deformation of sandstone, southern Appalachian fold-thrust belt, *Geol. Soc. Am. Bull.*, *103*, 861–875, doi:10.1130/0016-7606(1991)103<0861:LTDOSS>2.3.CO;2.
Wu, S. Z., K. T. Chau, and T. X. Yu (2004), Crushing and fragmentation of brittle spheres under double impact test, *Powder Technol.*, *143–144*, 41–55.
Zhang, J., T.-F. Wong, and D. M. Davis (1990), Micromechanics of pressure-induced grain crushing in porous rocks, *J. Geophys. Res.*, *95*(B1), 341–352, doi:10.1029/JB095iB01p00341.
Zoback, M. D., and J. D. Byerlee (1976), Effect of high-pressure deformation on permeability of Ottawa sand, *AAPG Bull.*, *60*(9), 1531–1542.

R. H. Brzesowsky, Philips Research, High Tech Campus 7, 5656 AE Eindhoven, Netherlands.
S. J. T. Hangx, Shell Global Solutions International, Kesslerpark 1, 2288 GS Rijswijk, Netherlands. (suzanne.hangx@shell.com)
C. J. Peach and C. J. Spiers, High Pressure and Temperature Laboratory, Faculty of Geosciences, Utrecht University, P.O. Box 80021, 3508 TA Utrecht, Netherlands.